nature portfolio

https://doi.org/10.1038/s41567-021-01476-w

Supplementary information

Realizing discontinuous quantum phase transitions in a strongly correlated driven optical lattice

In the format provided by the authors and unedited

Supplementary Information for Realizing discontinuous quantum phase transitions in a strongly-correlated driven optical lattice

Bo Song,[1] Shovan Dutta,[1] Shaurya Bhave,[1] Jr-Chiun Yu,[1] Edward Carter,[1] Nigel Cooper,[1,2] and Ulrich Schneider[1]

[1] *Cavendish Laboratory, University of Cambridge, J.J. Thomson Avenue, Cambridge CB3 0HE, United Kingdom*

[2] *Department of Physics and Astronomy, University of Florence, Via G. Sansone 1, 50019 Sesto Fiorentino, Italy*

(Dated: January 17, 2022)

Contents

I. Micromotion

The acceleration of the lattice gives rise to a periodic oscillation of all quasimomenta in the lattice frame. For atoms within a given band and with quasimomenta away from the Brillouin zone boundary, this micromotion is not observable in the lab frame, as it is precisely compensated by the transformation between the two frames of reference. For quasimomenta close to $\pm\hbar k_0$, however, the situation changes: Even a small-amplitude oscillation around the Brillouin zone boundary will give rise to Bragg reflections that transfer atoms between $+\hbar k_0$ and $-\hbar k_0$, which are mapped to opposite real momenta during time-of-flight imaging, thereby resulting in a strong oscillation of the center-of-mass position ($\propto \bar{k}_y$) observed after time of flight.

For a fixed modulation frequency f, the resulting oscillation in $\bar{k}_y$ would have the same frequency, i.e. $\bar{k}_y \propto \cos(2\pi f t)$. For more general sweeps, the final phase of the modulation can be written as $\phi(\tau) = 2\pi \int_0^\tau f(t)dt$, where the initial phase offset is set to $\phi(0) = 0$. In the sweep measurements, we vary the sweep duration τ during which the shaking frequency is linearly ramped from the initial frequency f_i to the final frequency f_f. This results in $\phi(\tau) = 2\pi \bar{f}\tau$, i.e. the final phase oscillates with the average shaking frequency $\bar{f} = (f_i + f_f)/2$. We experimentally confirm this by extracting the center of mass in momentum space from the normalized momentum distributions $n(k_y)$ shown in Fig. 4a in the main text according to $\bar{k}_y = \int k_y\, n(k_y) dk_y$. In Fig. S1, $\bar{k}_y$ is plotted as a function of sweep duration τ, and the oscillation frequency determined by a Voigt fit to its Fourier transform, $f_{peak} = 1.02\bar{f}$, is found to be equal to $\bar{f}$ within the experimental uncertainty.

II. Dephasing of superfluid correlations

To understand the nonzero value of $\partial\mathcal{N}_\pi/\partial\tau$ at weak shaking amplitudes in the backward sweep (from π-SF back to MI in Fig. 4b in the main text), we investigate the lifetime of the π-superfluid correlations in the shaken lattice. We prepare the system in the π-SF regime at a shaking frequency of 21kHz with different shaking amplitudes via the indirect sweep and then measure the evolution of $\mathcal{N}_\pi$ during a hold time t. We apply a linear fit to extract $\partial\mathcal{N}_\pi/\partial t$

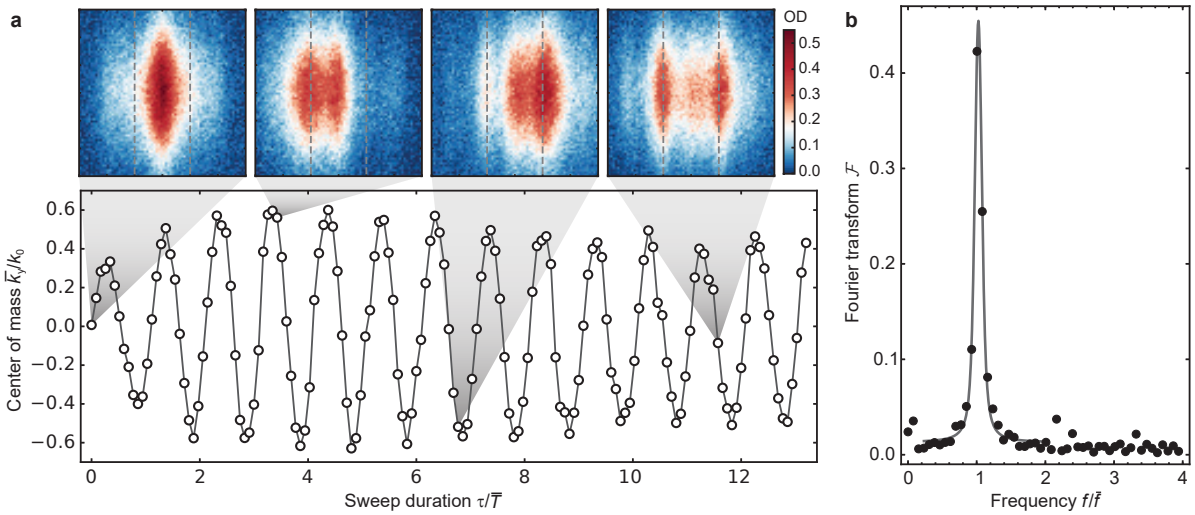

Figure S1. **Micromotion**. **a** Due to the combination of micromotion and Bragg reflections, the center of mass in momentum space oscillates as a function of the sweep duration τ. $\bar{T} = 1/\bar{f}$ denotes the average drive period with the average shaking frequency $\bar{f}$. The insets show examples of time-of-flight pictures for different sweep durations, highlighting the Bragg reflections between $\pm\hbar k_0$: In the lab frame, the population oscillates between these two discrete momenta, with equal populations at $\pm\hbar k_0$ coinciding with the times when the lattice has zero displacement. Dashed lines indicate $\pm\hbar k_0$. **b** The Fourier transform shows that the oscillation frequency is equal to the average shaking frequency $\bar{f}$. The line is a fit by a Voigt profile.

and, as shown in Fig. S2, find $\partial\mathcal{N}_\pi/\partial t = -65\,s^{-1}$, irrespective of the shaking amplitude $\mathcal{A}$. This incoherent dephasing produces a nonzero offset for $\partial\mathcal{N}_\pi/\partial\tau$ in the backward sweeps in Fig. 4 in the main text and is indicated there by the dashed line.

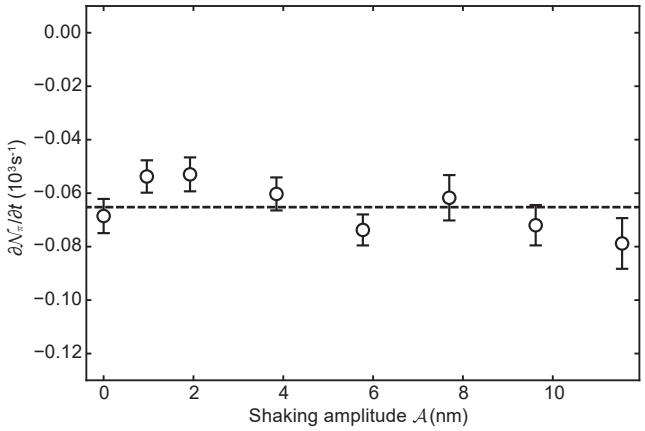

Figure S2. **Dephasing of superfluid correlations**. Rate of change of the band-edge population with respect to hold time, $\partial\mathcal{N}_\pi/\partial t$, measured for different shaking amplitudes $\mathcal{A}$. Error-bars indicate the standard error of each linear fit. The dashed line indicates the average decay rate.

III. Phase diagram and critical points

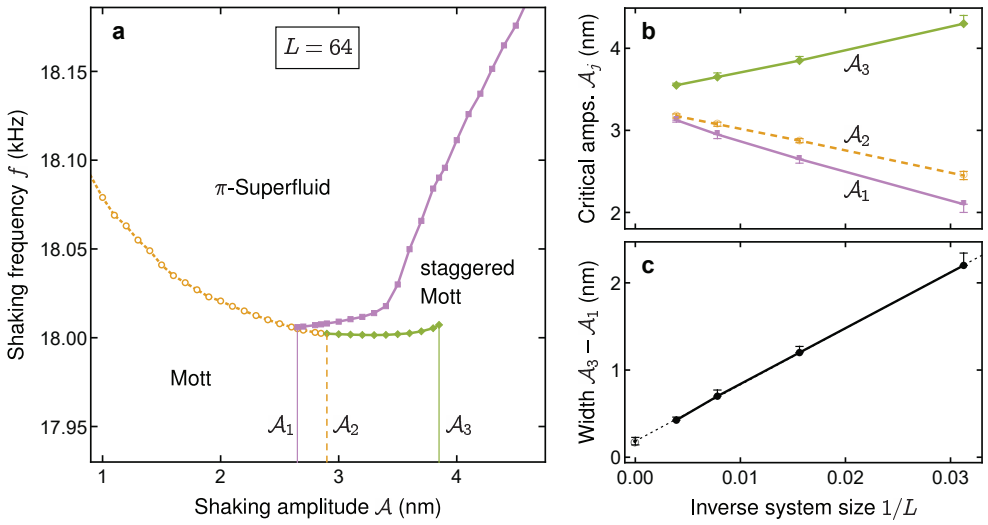

Figure S3. **Phase boundaries. a**, Phase diagram obtained by tracing the location of the jumps and peaks in the fitted CFT charge in Extended Data Fig. 2. The Mott to π-superfluid transition is discontinuous (first-order) for amplitudes $\mathcal{A} < \mathcal{A}_1$ (dashed yellow) and continuous for $\mathcal{A} > \mathcal{A}_1$ (solid blue). There is also a transition between non-staggered Mott and staggered Mott (alternating phases) for $\mathcal{A}_1 < \mathcal{A} < \mathcal{A}_3$ that is discontinuous for $\mathcal{A} < \mathcal{A}_2$ and continuous (solid green) for $\mathcal{A} > \mathcal{A}_2$. **b-c**, The interval $\mathcal{A}_1$-$\mathcal{A}_3$ shrinks as $1/L$, indicating the non-staggered to staggered Mott transition could be a finite-size effect.

Between amplitudes $\mathcal{A}_1$ and $\mathcal{A}_3$ in Fig. S3a, we find two closely-spaced phase transitions. The intermediate phase can be identified as a staggered Mott phase where the phase correlations alternate in sign, $\langle\langle \hat{a}_i^\dagger \hat{a}_{i+r} \rangle\rangle \sim (-1)^r e^{-r/\xi}$ (double brackets denote bulk averaging). At the non-staggered to staggered Mott transition, the band occupations are inverted (Fig. S4a), the nearest-neighbor correlation $\langle\langle \hat{a}_i^\dagger \hat{a}_{i+1} \rangle\rangle$ flips sign (Fig. S4b), and the density fluctuation in the lowest band reaches a maximum (Fig. S4e). For $\mathcal{A}_2 < \mathcal{A} < \mathcal{A}_3$, this transition is continuous and accompanied by a sharp peak in the density-density correlation length at the critical point (Fig. S4f). Above $\mathcal{A}_3$, this transition between non-staggered and staggered Mott insulators becomes a crossover. Furthermore, the 'phase transition' between different Mott states could be a finite-size effect, as the interval $\mathcal{A}_1$-$\mathcal{A}_3$ shrinks as $1/L$, see Figs. S3(b-c). This points to a simpler picture in the thermodynamic limit, where one only has a first-order non-staggered Mott to π-superfluid transition below a critical amplitude $\mathcal{A}^* \approx 3.3$ nm and a continuous staggered Mott to π-superfluid transition for $\mathcal{A} > \mathcal{A}^*$.

IV. Three-band simulations

So far we have considered only the lowest two bands and ignored the coupling to higher bands. In this section we include the third band and show that it has a significant effect on the dynamics only for large-amplitude sweeps over long periods of time. We extend the modeling in Methods by writing the field operator as

$$\hat{\psi}(y) = \sum_j w_1(y - y_j)\,\hat{a}_j + w_2(y - y_j)\,\hat{b}_j + w_3(y - y_j)\,\hat{c}_j\,, \tag{S1}$$

where $\hat{c}_j$ annihilates a particle at site y_j in the third (second-excited) band and w_3 is the corresponding Wannier function. Substituting this expansion into the lattice-frame Hamiltonian [Eq. (5)] and retaining the most significant terms for a deep lattice, we find

$$\hat{H}(t) = \hat{T} + \hat{U} + \hat{S}(t)\,, \tag{S2}$$

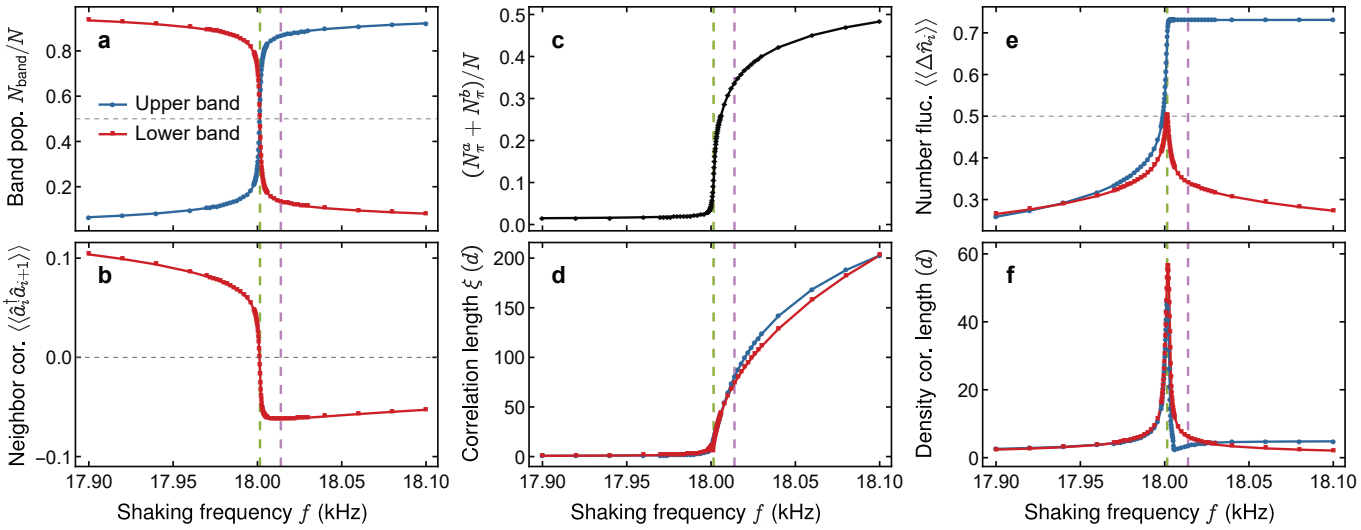

Figure S4. **Evolution of ground state across phase transitions**. Ground-state properties for $L = 64$ and $\mathcal{A} = 3.3$ nm as a function of the shaking frequency across back-to-back transitions from a non-staggered to a staggered Mott and from a staggered Mott to a π-superfluid (Fig. S3a). At the former, **a**, band populations are inverted, **b**, the nearest-neighbor correlation in the lowest band flips sign, **c**, populations at the band edge and **d**, single-particle correlation lengths start growing rapidly, **e**, number fluctuations are maximized, and **f**, density-density correlation length diverges (for $\mathcal{A}_2 < \mathcal{A} < \mathcal{A}_3$). The density correlation length is found by estimating where the correlation $\langle\langle \hat{n}_i, \hat{n}_{i+r}\rangle\rangle$ decays to a hundredth of its maximum value, where $\langle \hat{n}_i, \hat{n}_j\rangle := \langle \hat{n}_i \hat{n}_j\rangle - \langle \hat{n}_i\rangle\langle \hat{n}_j\rangle$.

where

$$\hat{T} := \sum_j (\varepsilon_a - \varepsilon_b)\,\hat{n}_j^a + (\varepsilon_c - \varepsilon_b)\,\hat{n}_j^c - J_a \sum_{\langle i,j\rangle} \hat{a}_i^\dagger \hat{a}_j + J_b \sum_{\langle i,j\rangle} \hat{b}_i^\dagger \hat{b}_j + J_b' \sum_{\langle\langle i,j\rangle\rangle} \hat{b}_i^\dagger \hat{b}_j + \sum_{r=1}^{r_{\max}} J_c(r)\big(\hat{c}_i^\dagger \hat{c}_{i+r} + \text{h.c.}\big)\,, \tag{S3}$$

$$\begin{aligned}\hat{U} := \sum_j &\frac{U_a}{2}\hat{a}_j^\dagger \hat{a}_j^\dagger \hat{a}_j \hat{a}_j + \frac{U_b}{2}\hat{b}_j^\dagger \hat{b}_j^\dagger \hat{b}_j \hat{b}_j + \frac{U_c}{2}\hat{c}_j^\dagger \hat{c}_j^\dagger \hat{c}_j \hat{c}_j + U_{ab}\hat{n}_j^a \hat{n}_j^b + U_{bc}\hat{n}_j^b \hat{n}_j^c + U_{ac}\hat{n}_j^a \hat{n}_j^c + U_{bb}^{ac}\big(\hat{a}_j^\dagger \hat{c}_j^\dagger \hat{b}_j \hat{b}_j + \text{h.c.}\big) \\ &+ \left(\frac{U_{ab}}{4}\hat{a}_j^\dagger \hat{a}_j^\dagger \hat{b}_j \hat{b}_j + \frac{U_{bc}}{4}\hat{b}_j^\dagger \hat{b}_j^\dagger \hat{c}_j \hat{c}_j + \frac{U_{ac}}{4}\hat{a}_j^\dagger \hat{a}_j^\dagger \hat{c}_j \hat{c}_j + U_{aa}^{ac}\hat{a}_j^\dagger \hat{n}_j^a \hat{c}_j + U_{cc}^{ac}\hat{a}_j^\dagger \hat{n}_j^c \hat{c}_j + 2U_{bb}^{ac}\hat{a}_j^\dagger \hat{n}_j^b \hat{c}_j + \text{h.c.}\right),\end{aligned} \tag{S4}$$

$$\hat{S}(t) := F(t) d \sum_j j\big(\hat{n}_j^a + \hat{n}_j^b + \hat{n}_j^c\big) + \alpha_{ab}\big(\hat{a}_j^\dagger \hat{b}_j + \hat{b}_j^\dagger \hat{a}_j\big) + \alpha_{bc}\big(\hat{b}_j^\dagger \hat{c}_j + \hat{c}_j^\dagger \hat{b}_j\big)\,, \tag{S5}$$

where ε_c is the average energy of the third band, $\hat{n}_j^x \equiv \hat{x}_j^\dagger \hat{x}_j$ denotes the on-site occupation in each band, and

$$\alpha_{ab} = \frac{1}{d}\int \mathrm{d}y\, y\, w_1(y) w_2(y)\,, \quad \alpha_{bc} = \frac{1}{d}\int \mathrm{d}y\, y\, w_2(y) w_3(y) \tag{S6}$$

give the coupling between the neighboring bands. Note there is no direct coupling between the first and the third band as those Wannier functions have the same parity and the shaking represents a linear potential in the lattice frame. For the experimental lattice depth $V_0 = 8.4E_r$, the tunneling amplitudes $J_c(r)$ fall off rapidly with separation r and we take $r_{\max} = 3$ in the simulations which accurately reproduces the band structure. As in Methods, we find the parameters $\varepsilon_b - \varepsilon_a = 19.7\,\text{kHz}$, $\varepsilon_c - \varepsilon_b = 17.1$ kHz, $J_a = 0.12\,\text{kHz}$, $J_b = 1.29\,\text{kHz}$, $J_b' = 0.17\,\text{kHz}$, $J_c(1) = -3.71\,\text{kHz}$, $J_c(2) = 0.45\,\text{kHz}$, $J_c(3) = -0.31\,\text{kHz}$, $U_a = 2.88\,\text{kHz}$, $U_b = 1.73\,\text{kHz}$, $U_c = 1.22\,\text{kHz}$, $U_{ab} = 2.36\,\text{kHz}$, $U_{bc} = 1.90\,\text{kHz}$, $U_{ac} = 1.49\,\text{kHz}$, $U_{bb}^{ac} = -0.38\,\text{kHz}$, $U_{aa}^{ac} = 0.91\,\text{kHz}$, $U_{cc}^{ac} = -0.12\,\text{kHz}$, $\alpha_{ab} = 0.15$, and $\alpha_{bc} = -0.23$. We simulate the experimental sweeps using adaptive tDMRG with the same numerical parameters as in Methods.

Figure S5 shows the evolution during such a sweep at relatively strong shaking amplitude ($\mathcal{A} = 5.8$ nm) where the shaking frequency f is swept through resonance from 15 kHz to 21 kHz over 0.8 ms. Only about 10% of the particles

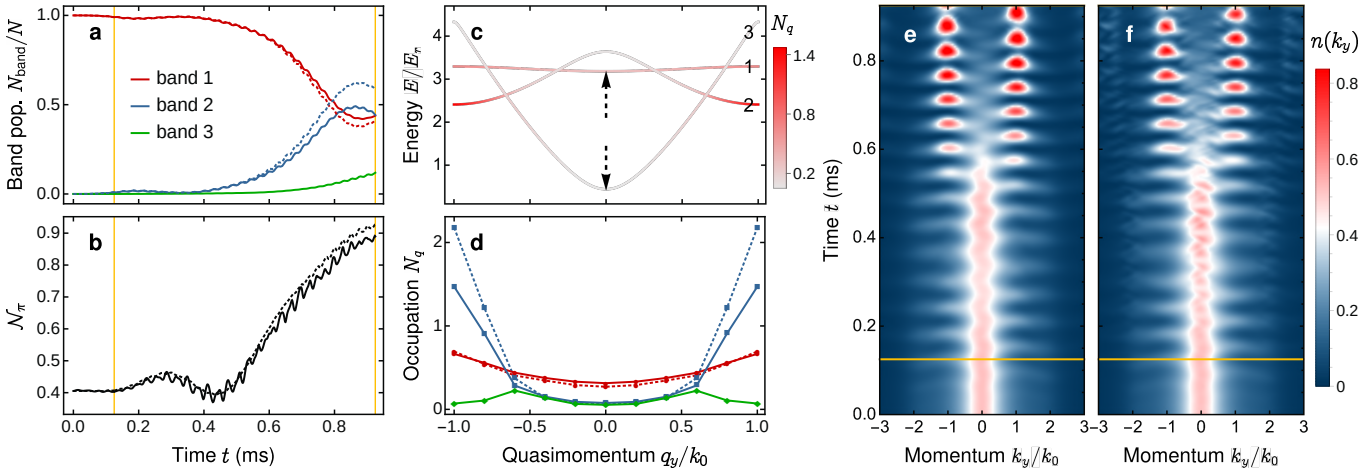

Figure S5. **Simulation of an experimental sweep.** tDMRG simulation of a two-step sweep sequence with $L = 10$, including the lowest two bands (dotted lines) and the lowest three bands (solid lines). First, the shaking amplitude $\mathcal{A}$ is ramped linearly from 0 to 5.8 nm over 0.125 ms (yellow grid line) with shaking frequency $f = 15\,\text{kHz}$. Next, f is swept linearly from 15 kHz to 21 kHz over $\tau = 0.8$ ms. **a**, Relative population of the bare bands, showing a small third-band excitation, and **b**, the resulting population $\mathcal{N}_\pi$. **c**, Occupation of bare bands in the rotating frame at the end of the sweep, where the first band is raised by hf and the third band is lowered by hf. Black arrows indicate the relative movement of these band during the sweep, highlighting that the third band is always off-resonant at the edge of the Brillouin zone. **d**, Final quasimomentum occupations showing sharp peaks at $\pm\hbar k_0$ and small peaks in the third band where it crosses the second band. These give rise to satellite peaks in the normalized momentum distribution, **f**, absent in a two-band simulation, **e**.

are excited to the third band toward the end of the sweep (Fig. S5a). As shown in Figs. S5(c-d), this excitation occurs primarily at quasimomenta where the second and third bands are resonant. Note the particles migrate from the first to the second band near the edge of the Brillouin zone, which remains off-resonant with the third band throughout the sweep. The small third-band population leads to satellite peaks in the plane-wave basis (Fig. S5f), as observed in the experiment (Fig. 1e) but absent in a two-band simulation (Fig. S5e). Thus, the observable $\mathcal{N}_\pi$ is slightly reduced by the presence of the third band (Fig. S5b). It also exhibits stronger oscillations at frequency $2f$. This frequency doubling arises because $\mathcal{N}_\pi$ is calculated by adding counter-propagating modes (see Extended Data Fig. 5a).

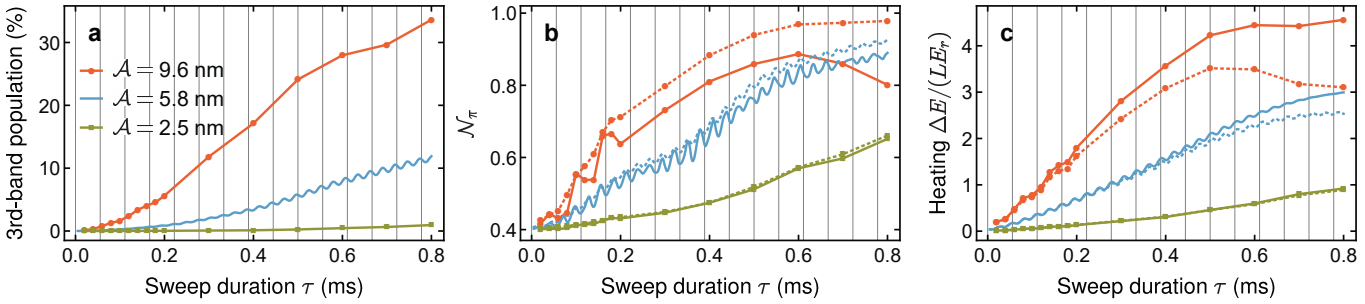

Figure S6. **Three-band vs two-band simulations**. Occupations and energies at the end of frequency sweeps with different amplitudes $\mathcal{A}$ and sweep durations τ, from two-band (dotted) and three-band (solid) simulations. **a**, Population of the third band grows with both $\mathcal{A}$ and τ. **b**, $\mathcal{N}_\pi$ is reduced and oscillates more strongly due to population transfer to the third band. **c**, Third-band excitation causes more heating (relative to the undriven Hamiltonian). Vertical lines are spaced by the average frequency $\bar{f} = 18$ kHz, showing that the fast oscillations occur at frequency $2\bar{f}$ due to micromotion (see Sec. I).

Figure S6 shows that the third band is more significant at larger shaking amplitudes and longer sweep durations. In particular, its population is less than 10% for amplitudes $\mathcal{A} < 5\,\text{nm}$ and practically zero for $\mathcal{A} < 2.6\,\text{nm}$ (Fig. S6a)

where the phase transition is discontinuous (Fig. S3a). Stronger shaking over a long period allows more particles to be transferred from the second to the third band, decreasing $\mathcal{N}_\pi$ (Fig. S6b) and causing more heating (Fig. S6c). Note that the energy is bounded for a finite number of bands, so the heating eventually saturates as longer sweeps become adiabatic. Figure S6b shows that as a function of the sweep duration, the final value of $\mathcal{N}_\pi$ exhibits fast oscillations at twice the average shaking frequency (for linear ramps from 15 to 21 kHz), which originates from the fast oscillations in its time evolution (Fig. S5b). $\Omega \propto f^2\mathcal{A}$